Journal of Statistical Physics, Vol. 62, Nos. 5/6, 1991

Nonequilibrium Brownian Dynamics Simulations of Shear Thinning in Concentrated Colloidal Suspensions

Gerald Wilemski[1]

Received February 2, 1990; final September 28, 1990

The effect of interparticle forces on shear thinning in concentrated aqueous and nonaqueous colloidal suspensions was studied using nonequilibrium Brownian dynamics. Hydrodynamic interactions among particles were neglected. Systems of 108 particles were studied at volume fractions ϕ of 0.2 and 0.4. For the nonaqueous systems, shear thinning could be correlated with the gradual breakup of small flocs present because of the weak, attractive secondary minimum in the interparticle potential. At the highest shear rate for $\phi = 0.4$, the particles were organized into a hexagonally packed array of strings. For the strongly repulsive aqueous systems, the viscosity appeared to be a discontinuous function of the shear rate. For $\phi = 0.4$, this discontinuity coincided with a transition from a disordered state to a lamellar structure for the suspension.

KEY WORDS: Colloidal suspensions; viscosity; shear thinning; Brownian dynamics.

1. INTRODUCTION

Colloidal suspensions exhibit many interesting equilibrium and nonequilibrium properties. In equilibrium suspensions, for example, particles can be found in gas-, liquid-, or solidlike phases depending on temperature, density, and particle/medium characteristics. The rheological behavior of these suspensions is also very complex with non-Newtonian behavior such as shear thinning, shear thickening, dilatancy, and thixotropy commonly occurring. A recent volume reviews many aspects of the field.[1]

This paper presents the results of nonequilibrium Brownian dynamics (NEBD) simulations performed to study shear thinning in simple, model

[1] Physical Sciences Inc., 20 New England Business Center, Andover Massachusetts 01810.

0022-4715/91/0300-1239$06.50/0

aqueous and nonaqueous colloidal suspensions. Shear thinning is simply the decrease in the apparent viscosity of the suspension with increasing shear rate. Although there have been numerous investigations of the shear viscosity of molecular fluids using nonequilibrium molecular dynamics (NEMD) techniques, there are only a few computer simulation studies directly concerned with the shear rate dependence of the viscosity of colloidal suspensions. Using NEMD techniques, Evans and Watts[2] found modest shear thinning and dilatancy for the screened Coulomb potential often used to model lyophobic suspensions. Using Stokesian dynamics simulations, Brady and Bossis[3-5] have extensively investigated the effects of hydrodynamic interactions on the viscosity of monolayer suspensions. Hydrodynamic interactions alone produce no shear thinning, but do result in modest shear thickening at higher shear rates when either strong repulsive forces or Brownian motion are included in the simulations. With Brownian motion included, shear thinning is also found. Woodcock[6] has shown that with appropriate choices of time and length scales, NEMD results for soft spheres (r^{-12} potential) agreed well with experimental measurements of shear thinning for two different nonaqueous monodisperse suspensions. Woodcock[6] has also identified an interesting transition between amorphous and layered phases in the viscosity versus shear rate curve for the soft-sphere system. Heyes[7,8] has reported ordered structure formation and shear thinning at several volume fractions in NEBD simulations of the soft-sphere (r^{-12}) system. Finally, Doi and Chen[9] have recently simulated sheared aggregating colloids using a sticky sphere model with deterministic particle motion governed by hydrodynamics. Their 2D simulations neglected hydrodynamic interactions and qualitatively reproduced key rheological features observed experimentally.

While the NEMD results are interesting and instructive, the NEMD technique does not strictly represent the dynamics of colloidal particles in a suspension, nor is the soft-sphere potential a realistic potential for colloidal particles, i.e., derivable from the physics of interacting colloidal particles. Also, while the monolayer and 2D simulations are valuable and interesting, their direct applicability to three-dimensional systems is not yet strongly established. The only investigations of 3D colloidal suspension viscosity using Brownian simulation methods known to me are those of Heyes[7,8] and my own preliminary study.[10] Given this background, it seems reasonable to ask what effect the type of colloidal interparticle potential has on the magnitude of the shear viscosity and on its shear rate dependence. This question motivates the present work. Previous work indicates that there should be significant effects.[11]

2. SIMULATION METHODOLOGY

The simulations were performed using the Brownian dynamics algorithm originally devised by Ermak and McCammon[12] and Fixman[13] with a shear flow term added.[10,14] Periodic boundary conditions and the coordinate space version[3-5] of the homogeneous shear conditions introduced by Lees and Edwards[15,16] were used to simulate shearing of an infinite system with continuous flow fields across cell boundaries. A simple shear flow in the x direction was used; the imposed velocity flow field acting on a particle with a given y coordinate was given by $u_x = \dot{\gamma} y$, where $\dot{\gamma}$ is the shear rate ($\sec^{-1}$).

The main focus of this study was the effect of interparticle colloidal forces on shear thinning, and hydrodynamic interactions among particles were neglected. Systems of 108 spherical particles of diameter $d = 1.2\ \mu$m were simulated at two volume fractions ($\phi = 0.2, 0.4$). Pair potentials appropriate for particles in aqueous and nonaqueous media were used. The pair potential for the nonaqueous system was the sum of an attractive interaction due to van der Waals forces[17] u_A and a steeply repulsive interaction due to polymeric steric repulsion[18] u_S:

$$u_A(r) = -A\{(d/r)^2 - [1-(r/d)^2]^{-1} + 2\ln[1-(d/r)^2]\}/12 \tag{1}$$

$$u_S(r) = kTS(2R_0 + r)(R_0 - r)^2 \tag{2}$$

Here, r is the distance between particle centers, and R_0 ($= d + 2\delta$) is the range of the steric repulsive potential, where $\delta(0.02\ \mu\text{m})$ is the thickness of the adsorbed polymer layer. Also, k is the Boltzmann constant, T (293 K) is the absolute temperature, A (5.0×10^{-20} J) is the Hamaker constant, and S ($5.82 \times 10^{16}\ \text{cm}^{-3}$) is a composite parameter that controls the strength of the steric repulsion. The value for S is based on parameters[10,19] for poly(12-hydroxystearic acid) chains in a dodecane solvent, with a concentration of 0.013 g/cm^3 of polymer segments per unit volume of adsorbed layer. Although the repulsive barrier of this potential is quite high (154 kT at $r/d = 1.0055$), to ensure that trapping in the primary minimum, i.e., irreversible coagulation, could not occur, the absolute value of the force derivable from Eqs. (1) and (2) was used for $r/d < 1.0055$.

For the aqueous systems, only the highly dominant repulsive potential due to the overlap of electrical double layers was retained. The range of these pair interactions is characterized by the familiar Debye screening length κ^{-1}. The specific form used was that recommended by Verwey and Overbeek[20,21] for particles interacting with constant surface potential in electrolytes of high ionic strength, $\kappa d \geq 3$:

$$u_D(r) = \pi\varepsilon\psi_0^2 \ln\{1 + \exp[-\kappa(r-d)]\} \tag{3}$$

where ε (7.08×10^{-10} F/m) is the aqueous electrical permittivity, and ψ_0 (0.06 V) is the electrical potential at the particle surface. Simulations with this potential were run at two electrolyte concentrations (10^{-4} and 10^{-6} mole/dm^3) giving values for κd of 39.4 and 3.94, respectively.

The average stress due to interacting particles was computed from the formula

$$\sigma_{xy} = -V^{-1} \left\langle \sum\sum_{i>j} y_{ij} F_{xij} \right\rangle \tag{4}$$

where F_x is the x component of the force between particles i and j, V is the system volume, and $\langle \cdot \rangle$ denotes a time average. The increment in viscosity due to the interparticle stress is obtained as $\Delta\eta = \sigma_{xy}/\dot{\gamma}$. The apparent viscosity of the suspension differs from $\Delta\eta$ by the viscosity of the pure suspending fluid, η_0 (10^{-3} Pa · sec), and another additive term that, with the neglect of hydrodynamic interactions, depends only on ϕ. The pair correlation function $g(r)$ was computed by counting pairs in intervals of width $\Delta r = d/40$. Although structural deformation of colloidal suspensions occurs under the influence of shear, giving rise to an angular dependence in $g(r)$,[22] only spherically averaged values for g were computed in order to reduce the computational effort.

The systems were studied over shear rates of 5–400 sec^{-1}, thus varying the influence of Brownian motion and convective flow due to shear on the particle dynamics. The Peclet number Pe provides a measure of the relative importance of these two effects, since it is a ratio of characteristic times for diffusive and convective displacements of particles. Here, Pe is defined as $6\pi\eta_0 a^3\dot{\gamma}/kT$, where $a = d/2$, and it numerically equals $\dot{\gamma}$ for the values of η_0, d, and T employed here.

Generally, runs at a given shear rate were begun using the particle coordinates from the end of a run at a different, but usually nearby, shear rate. Typically 10,000–20,000 time steps were then used to bring the system to a steady state at the new shear rate before averaging was begun. For the first run with each system, the particles were placed on the sites of an fcc lattice. Without shear each of the two strongly repulsive aqueous systems ($\phi = 0.4$ and $\phi = 0.2$ with $\kappa d = 3.94$) maintained a broadened fcc structure over long simulation runs. Application of shear to these systems effectively produced shear-induced melting. The nonaqueous systems were disordered at equilibrium.

3. RESULTS

The average viscosity increments $\Delta\eta$ are plotted versus shear rate $\dot{\gamma}$ in Fig. 1. The results are grouped by volume fraction. Conditions for each run

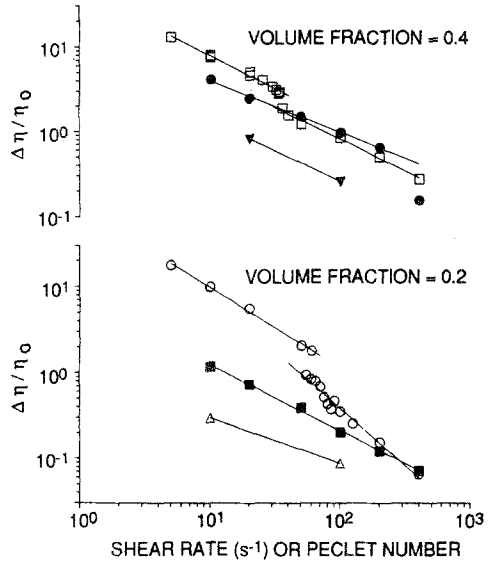

Fig. 1. Shear rate dependence of the relative viscosity increment. Aqueous suspensions: (□) $\kappa d = 39.4$; (○) $\kappa d = 3.94$; (△) $\kappa d = 39.4$; Nonaqueous suspensions: (●) $A/kT = 12.4$; (■) $A/kT = 12.4$; (▼) $A/kT = 0$. The lines are least-squares fits to the equation $\Delta\eta \propto \dot{\gamma}^{-p}$; values for p are for the indicated ranges of shear rates: (□) 0.77, 5–34 sec^{-1}; 0.75, 36–200 sec^{-1}; (○) 0.94, 5–60 sec^{-1}, 1.34, 55–400 sec^{-1}; (△) 0.53, 10–100 sec^{-1}; (●) 0.61, 10–200 sec^{-1}; (■) 0.77, 10–400 sec^{-1}; (▼) 0.72, 20–100 sec^{-1}.

are summarized in Table I. The viscosity increment displays an inverse power law dependence on $\dot{\gamma}$, $\Delta\eta \propto \dot{\gamma}^{-p}$. The values for p are noted in the caption to Fig. 1; they are significantly larger than those reported by Heyes[7,8] for the soft-sphere system. This supports the notion that the nature of the interparticle force has an appreciable influence on the degree of shear thinning.

The most obvious feature in plot is the apparent discontinuity in $\Delta\eta$ vs. $\dot{\gamma}$ for each of the strongly interacting aqueous systems. I investigated the case with $\phi = 0.4$ more thoroughly and will focus on it. For this system, the discontinuity occurs for $34 < \mathrm{Pe} < 36$. For $\mathrm{Pe} \leqslant 34$ the system exhibited very large fluctuations in the stress as seen in Fig. 2, where values of $\Delta\eta$, averaged over successive intervals of $(\dot{\gamma}\,\Delta t)^{-1}$ steps, are plotted versus time. The high fluctuation level in the low-shear-rate "trajectories" stands in sharp contrast to the relatively quiet behavior of the system at $\mathrm{Pe} \geqslant 36$. We should note that the runs at $\mathrm{Pe} = 34$ and 36 were each started (with no preliminary equilibration) with the *same* set of particle coordinates taken from the end of the run at $\mathrm{Pe} = 40$. This makes the disparity in appearance even more striking. The run at $\mathrm{Pe} = 32$ was begun with coordinates from

Table I. Summary of NEBD Simulations[a]

Aqueous, $\phi = 0.4$, $\kappa d = 39.4$																	
$\dot{\gamma}$ (sec^{-1})	5	10	10	20	20	25	30	32	$33\frac{1}{3}$	34	36	36	40	50	100	200	400
$\Delta t \times 10^5$ (sec)	1	1	0.5	1	0.5	1	5/6	25/32	1	25/34	25/36	25/36	1	1	1	1	1
$n/1000$	160	220	160	200	400	280	320	560	345	360	120	160	60	70	60	90	30
$\Delta\eta/\eta_0$	13.0	7.54	7.97	5.08	4.63	4.10	3.39	3.13	2.81	2.94	2.08	1.73	1.55	1.21	0.83	0.49	0.28
Nonaqueous, $\phi = 0.4$, $A = 5 \times 10^{-20}$ J																	
$\dot{\gamma}$ (sec)	10	20	50	100	200	400											
$\Delta t \times 10^6$ (sec)	5	5	5	5	5	5											
$n/1000$	40	30	28	40	40	30											
$\Delta\eta/\eta_0$	4.14	2.46	1.48	0.96	0.64	0.15											
Nonaqueous, $\phi = 0.4$, $A = 0$																	
$\dot{\gamma}$ (sec^{-1})	20	100															
$\Delta t \times 10^6$ (sec)	5	5															
$n/1000$	30	30															
$\Delta\eta/\eta_0$	0.81	0.26															
Aqueous, $\phi = 0.2$, $\kappa d = 3.94$																	
$\dot{\gamma}$ (sec^{-1})	5	10	20	50	60	55	60	65	70	75	80	85	90	100	125	200	400
$\Delta t \times 10^5$ (sec)	1	1	1	1	10/9	10/11	10/9	20/13	10/7	4/3	5/4	20/17	10/9	1	1	1	1
$n/1000$	40	60	90	70	240	60	90	80	120	120	80	40	40	80	40	30	40
$\Delta\eta/\eta_0$	17.6	9.87	5.58	2.05	1.80	0.93	0.85	0.80	0.69	0.52	0.43	0.38	0.47	0.35	0.25	0.15	0.066
Aqueous, $\phi = 0.2$, $\kappa d = 39.4$																	
$\dot{\gamma}$ (sec^{-1})	10	100															
$\Delta t \times 10^5$ (sec)	1	1															
$n/1000$	30	30															
$\Delta\eta/\eta_0$	0.30	0.088															
Nonaqueous, $\phi = 0.2$, $A = 5 \times 10^{-20}$ J																	
$\dot{\gamma}$ (sec^{-1})	10	20	50	100	200	400											
$\Delta t \times 10^6$ (sec)	5	5	5	5	5	5											
$n/1000$	40	30	30	30	30	30											
$\Delta\eta/\eta_0$	1.17	0.73	0.39	0.20	0.12	0.072											

[a] Listed are the volume fraction ϕ, Debye parameter κd, Hamaker constant A, shear rate $\dot{\gamma}$, time step Δt, number of steps per run n, and the run-average relative viscosity increment $\Delta\eta/\eta_0$.

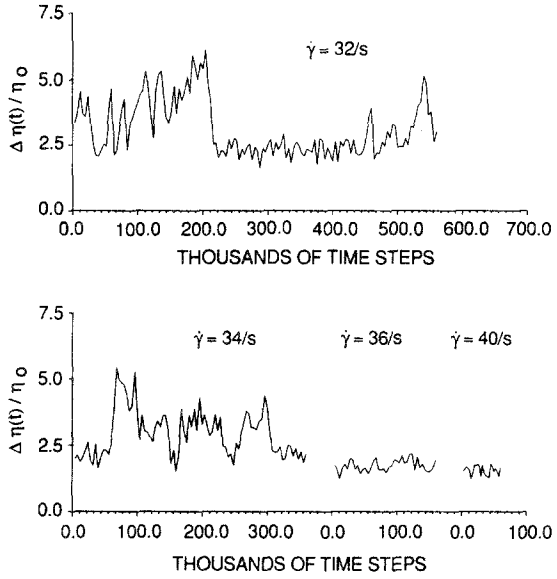

Fig. 2. Time dependence of the relative viscosity increment for concentrated aqueous suspensions ($\phi = 0.4$, $\kappa d = 39.4$) at several shear rates. The curve is generated by dividing the run into intervals of $1/(\dot{\gamma}\,\Delta t)$ steps and connecting the average values for successive intervals with straight-line segments.

a Pe = 30 state, and it shows definite signs of bistability. In contrast, the run at Pe = 30 (not shown), which started with Pe = 25 coordinates, was also characterized by large fluctuations, but it showed no long-lived excursions below $\Delta\eta/\eta_0 = 2.5$, as did its offshoot. A long run at Pe = 33.3 (not shown), which started with Pe = 20 coordinates, also showed signs of bistability.

The bistable nature of the system for $32 \leqslant \mathrm{Pe} \leqslant 34$ is illustrated in Fig. 3. These snapshots show entire sets of particle coordinates, selected at specific times, projected onto the yz plane. The shear flow is directed into the page, and the velocity gradient is in the y direction. Figure 3a shows a configuration taken from the low-stress region for Pe = 32 after 320,000 steps, and Fig. 3b shows the projected particle configuration at the end of the Pe = 34 run, also a low stress state. The lamellar structure of the suspension is evident in these two shots. In contrast, Fig. 3c shows a disordered particle configuration for a high-stress state after 80,000 steps at Pe = 34.

Despite the recurring presence of the lower-stress lamellar states, the overall average value of the stress is dominated by the disordered states. This is reflected in the values plotted in Fig. 1 and listed in Table I, which

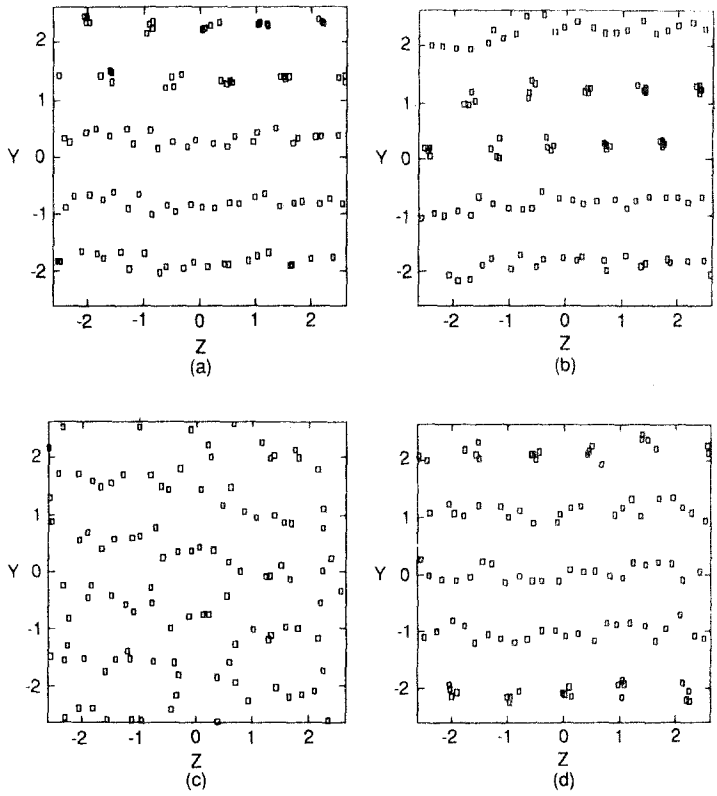

Fig. 3. Snapshots of particle configurations projected onto the plane normal to the flow for aqueous suspensions with $\phi = 0.4$, $\kappa d = 39.4$, at several shear rates. Each symbol locates the center of a particle. Axis dimensions are scaled by the particle diameter. Shear rates (sec $^{-1}$): (a) 32, (b) 34, (c) 34, (d) 36.

were obtained by averaging over the entire run rather than by separately averaging over the high- and low-stress regions. I based this procedure on the argument that the real time spent by the system in one state or the other ($\leqslant 1$ sec) was short compared to the time in which macroscopic measurements of viscosity could generally be made. Thus, the measurement would also average over fluctuations.

Figure 3d shows the stable lamellar structure found for the Pe = 36 run that began with Pe = 40 coordinates. To check the stability of the system at Pe = 36, a second run of 120,000 steps was made starting with the end configuration of the Pe = 34 run. The results were very similar to those of the earlier run. The stress history showed the same low level of fluctuation, although the average value of $\Delta\eta$ was about 20% higher. The weighted average of the two runs was used in Fig. 1. On the basis of these

two runs, the stability of the system at Pe = 36 seems to be independent of the direction used to reach it.

The lamellar structure illustrated in Fig. 3 is stable for all shear rates from 36 to 400 sec^{-1}. It is interesting that, in each lamellar phase I observed, two of the layers are further organized into strings of particles along the fluid streamlines. The string layers occur in pairs with a triangular ordering of the strings. The particles in each layer (string or regular) are packed in distorted planar hexagonal arrays (with occasional defects). The hexagonal pattern of the string layers is stretched slightly in the flow direction while the deformation of the other layers is equivalent to about a 12° in-plane skewing of the string layer pattern away from the flow axis. A given layer could be skewed either positively or negatively.

These interesting structural changes do not show up very prominently in the spherically-averaged pair correlation functions. Figure 4 shows $g(r)$ for Pe = 36 and $g(r) + 0.5$ for Pe = 34. The inset figure shows the difference in $g(r)$ for several pairs of shear rates. The very small differences for Pe = (30, 34) and (36, 40) are typical. Generally, the effect of increasing

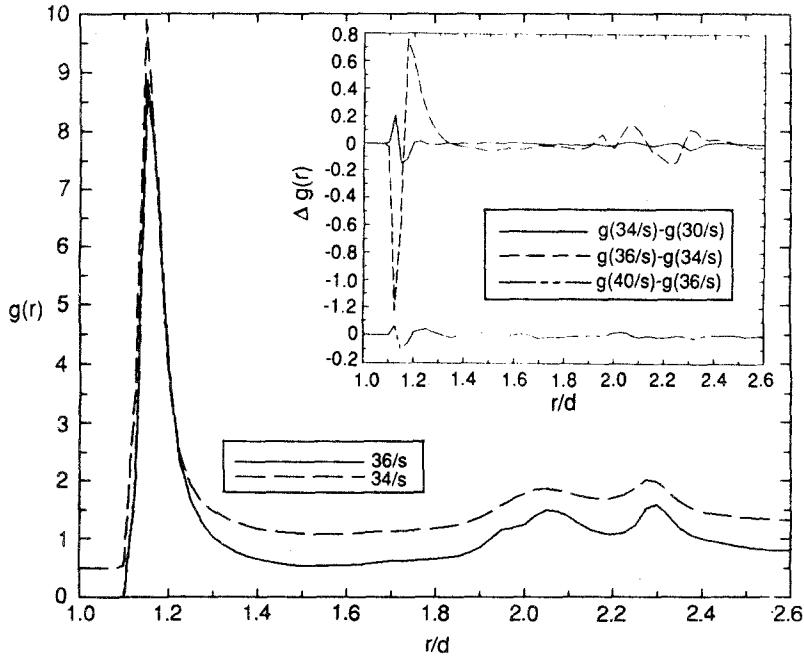

Fig. 4. Spherically-averaged pair correlation functions for aqueous suspension with $\phi = 0.4$, $\kappa d = 39.4$ at shear rates of 34 and 36 sec^{-1}. For 34 sec^{-1}, $g(r)$ is offset by 0.5 for clarity. Inset shows the differences between $g(r)$ at different shear rates.

shear rate is to shove particles slightly closer together on average, thereby producing a higher average stress. The transition to the lamellar phase results in a slight increase in the average nearest neighbor separation, as seen in the inset figure for $g(36\ \text{sec}^{-1}) - g(34\ \text{sec}^{-1})$, and this leads to a lower stress. The small changes in $g(r)$ at larger r do not contribute to the average stress, but are still indicative of the change in structure. These features are present for all $\dot{\gamma}$ out to $400\ \text{sec}^{-1}$. Figure 5 compares $g(r)$ at $\text{Pe} = 10$ and 200. In this case, the effect of shear on the nearest neighbor separation is quite evident. The inset to Fig. 5 compares $g(r)$ at $\text{Pe} = 10$ with $g(r)$ for a "quenched" suspension obtained by allowing a particle configuration characteristic of the $\text{Pe} = 10$ state to reequilibrate with no shear rate applied. The increase in the nearest neighbor distance of the "crystallized" suspension is evident. Judging by the locations of the peaks relative to the nearest neighbor peak, the static structure corresponds to an imperfect hcp lattice.

Two aqueous suspensions were studied with $\phi = 0.2$ primarily to simulate the secondary electroviscous effect.[11] To do this, the ionic

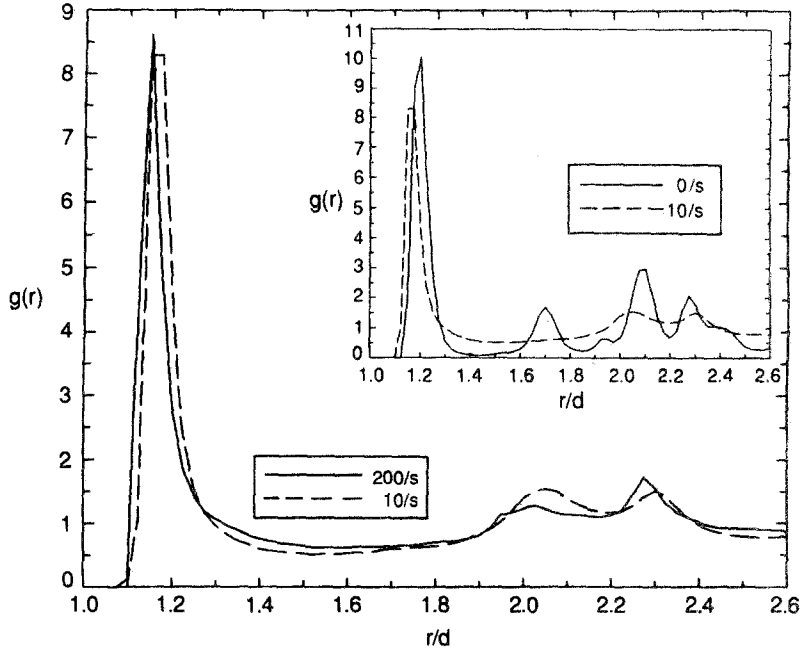

Fig. 5. Spherically-averaged pair correlation functions for aqueous suspension with $\phi = 0.4$, $\kappa d = 39.4$ at high and low shear rates. Inset compares $g(r)$ for low shear rate with $g(r)$ for the same suspension after equilibrating at zero shear rate.

strength of the suspending fluid was changed from 10^{-4} to 10^{-6} mole/dm^3. The reduction of ionic strength results in a tenfold jump in the Debye length, increasing the range of the repulsive force, and making the suspended particles interact more strongly. The effect of this is to significantly increase the suspension viscosity. The simulations qualitatively reproduce this effect, as Fig. 1 shows. Only two runs were made at the higher ionic strength, but these were sufficient for the comparison. The simulation results for $\Delta\eta/\eta_0$ of the low-ionic-strength system show a discontinuity similar to that of the more concentrated suspension. To explore this behavior, two series of runs were made, one with decreasing shear rate and the other with increasing shear rate. In contrast to the results at $\phi = 0.4$, in this case it was possible to find regions of shear rate where the high and low branches of the $\Delta\eta/\eta_0$ curves overlapped, although this may be due to insufficient run time for the cases on the lower branch. The entry at $\dot{\gamma} = 55\ \text{sec}^{-1}$ in Table I was the last "stable" state in the sequence of runs at decreasing shear rate. In the next run (result not plotted in Fig. 1 or listed in Table I) at $\dot{\gamma} = 50\ \text{sec}^{-1}$, $\Delta\eta/\eta_0$ slowly approached the upper curve, but the run was terminated after 160,000 steps before completing the transition. On the upper branch, with increasing shear rate, the last stable state was at $\dot{\gamma} = 60\ \text{sec}^{-1}$ for a run of 240,000 steps. Subsequent runs at $\dot{\gamma} = 67$ and $65\ \text{sec}^{-1}$ resulted in rapid transitions to the lower branch. (To reduce confusion, these results have also been omitted from Fig. 1 and Table I.) These transients seem to resemble those described by Woodcock.[6] In view of this shear thinning behavior, it would be surprising if this suspension failed to have ordered structures. In a cursory check of two states, I found ordered structures on each branch. On the upper branch at $\text{Pe} = 60$, one yz projection revealed a lamellar structure with layers slightly tilted with respect to the xz shear planes. At $\text{Pe} = 70$ on the lower branch, a lamellar structure resembling those in Fig. 3 was present.

Let us now consider the results for the nonaqueous suspensions, which are structurally very different from the aqueous suspensions. The attractive van der Waals force plays a major role here because of the very short range ($1.033d$) of the steric repulsive potential. At equilibrium, these suspensions are weakly aggregated into flocs with little long-range order. This is due to the weak, attractive secondary minimum (depth $\simeq 10kT$) in the interparticle potential. The attractive tail of this potential is nonzero out to about $1.1d$. Figure 6 shows $g(r)$ at $\text{Pe} = 400$, $2 + g(r)$ at $\text{Pe} = 100$, and $4 + g(r)$ at $\text{Pe} = 10$. For each of these spherically averaged pair correlation functions, there is a strong, localized peak at $r = 1.05d$ due to the attractive force. The inset shows what happens to $g(r)$ at $\text{Pe} = 100$ when the attractive force is shut off ($A = 0$): The nearest neighbor peak drops, broadens considerably, and the maximum moves outside of the range of the remaining repulsive

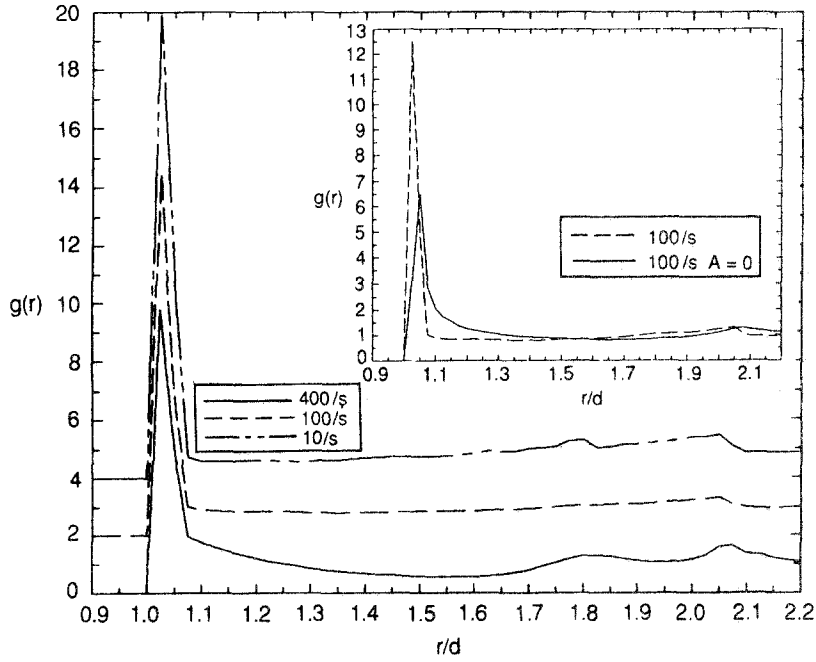

Fig. 6. Spherically-averaged pair correlation functions for nonaqueous suspensions for $\phi = 0.4$ at three different shear rates. For 100 and 10 sec^{-1}, $g(r)$ is offset by 2.0 and 4.0, respectively, for clarity. Inset shows the effect on $g(r)$ of turning off the attractive potential.

potential. The number of nearest neighbors between $1.013d$ and $1.088d$ also drops from 4.7 to 3.3. By holding particles closer together, the attractive force has a significant effect on the viscosity of the suspension. This can be seen in Fig. 1 by comparing the results with $(A/kT = 12.4)$ and without $(A = 0)$ the attractive force for $\phi = 0.4$.

Increasing the shear rate also has interesting effects on the structure of these suspensions. The first effect is the steady breakup of the small flocs formed because of the attractive force. At equilibrium the average number of nearest neighbors $(1.013 < r/d < 1.088)$ is 6.3. With increasing shear rate this number steadily declines: At Pe = 10, 20, 50, 100, 200, and 400, the respective numbers of nearest neighbors are 6.0, 5.5, 5.1, 4.7, 4.4, and 4.3 for $\phi = 0.4$, and 5.1, 4.4, 3.9, 2.8, 2.2, and 1.9 for $\phi = 0.2$. In contrast, for $\phi = 0.4$ with no attractive force present, the number of nearest neighbors between $1.013d$ and $1.088d$ remains essentially constant at 3.3 between Pe = 20 and 100.

A second effect of increasing shear rate is the reorganization of the particles into strings oriented along the fluid streamlines. This is illustrated

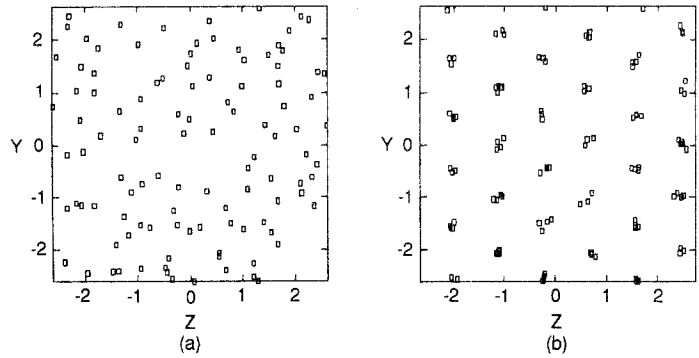

Fig. 7. Snapshots of particle configurations projected onto the plane normal to the flow for a nonaqueous suspension with $\phi = 0.4$ at shear rates of (a) 10 and (b) 400 sec^{-1}. Each symbol locates the center of a particle. Axis dimensions are scaled by the particle diameter.

in Fig. 7 by the two snapshots of particle configurations at $\phi = 0.4$. As in Fig. 3, these shots are projections of the centers of all particles onto yz plane. Figure 7a shows a disordered configuration that is typical at $Pe = 10$, while Fig. 7b reveals the dramatic reorganization of the particles into the hexagonally packed array of strings. A similar phenomenon has been found previously by Heyes[7,8] for the colloidal soft-sphere system. This structural reorganization accounts for the failure, in Fig. 1, of the simulation viscosity at $Pe = 400$ ($\phi = 0.4$) to lie on the same curve as the lower shear rate points. The apparent discrepancy is explained by the reduction in stress due to the structural change. At $Pe = 200$ a slight tendency to form strings was noted, but the suspension was largely disordered, and $g(r)$ was very similar to $g(r)$ at $Pe = 100$ (Fig. 6). At $Pe = 400$, $g(r)$ has developed some new characteristics indicative of the string phase, although the changes are not very dramatic.

Without the attractive force, string formation seems to be somewhat more favored. A snapshot at $Pe = 100$ of the purely repulsive nonaqueous suspension revealed one group of strings, several isolated strings, some partially layered sections, and disordered regions. A snapshot of the less concentrated ($\phi = 0.2$) nonaqueous suspension at $Pe = 400$ showed it to be largely disordered, although a few strings were present.

4. CONCLUSIONS

These simulations provide evidence for the importance of the interparticle potential in determining the behavior of sheared, simple colloidal suspensions, at least on a computer. The magnitude and shear rate dependence of the viscosity were found to depend on the type and strength

of the potential used. The simulations revealed many interesting features, such as the lamellar and string phases and discontinuous or abrupt shear thinning due to a structural transition, that have analogues in earlier NEMD simulations[6,23,24] and recent NEBD simulations.[7,8] These phenomena will undoubtedly provide many opportunities for future research.

However, recent work by Evans and Morriss[25] regarding the influence of thermostatting on NEMD simulation results provides a note of caution regarding the interpretation and applicability of simulation results to real systems. Although, as Heyes[8] has noted, NEBD simulations do not require thermostatting and the shear flows for colloidal fluids are low-Reynolds-number flows, we should still be conservative in our evaluation of these types of results until more is known about the effects of system size, boundary conditions, and simulation algorithms on the results. For example, computations currently in progress[26] for 256-particle systems tentatively suggest that the high-stress (low-Pe) branches of the shear thinning curves for the aqueous suspensions reported here may be only a metastable state in the larger system or may occur only at lower shear rates than so far studied.

Finally, one may question whether the inclusion of hydrodynamic interactions (HI) would affect the results reported here. HI were neglected, not out of any sense that they were unimportant, but solely for practical reasons. Their inclusion greatly complicates the algorithm for computing particle trajectories and necessitates a major increase in cpu time. Since I do not know of any 3D simulations of a sheared colloidal suspension with HI, I offer some remarks based on recent results for monolayer suspensions with HI.[3,5]

In these simulations, Bossis and Brady found qualitatively similar shear thinning behavior for a system of hard spheres and for a moderately repulsive screened Coulomb system with, at most, $O(1)$ differences in the relative viscosities for the two systems.[4] The contribution of HI to the relative viscosity was itself found to be of $O(1)$, and it increased rather slowly with increasing Peclet number for $\mathrm{Pe} > 1$.[4,5] The principal contribution to the hydrodynamic stress arose from configurations in which particles were nearly touching, as seen from $g(r)$ for the hard-sphere system.[5] The aqueous repulsive potentials used here prevent such small interparticle distances from occurring, so we might expect the magnitude of the hydrodynamic stress to be reduced somewhat from the values found for hard spheres. Because of the much shorter range of the nonaqueous potential, particles approach each other much more closely than in the aqueous systems, although still not as closely as in the hard sphere system. We might therefore expect a somewhat larger [but still $O(1)$] contribution to

the viscosity from HI for the nonaqueous system. It is also possible that the long range of the HI could promote structural ordering at lower shear rates and thus indirectly influence the viscosity by changing the interparticle force contribution to the average stress, Eq. (4).

ACKNOWLEDGMENTS

The early phases of this work were supported by AFOSR and Physical Sciences Inc. I thank Dr. R. Cook and Dr. A. Gelb for helpful discussions and J. E. Baker and Dr. A. A. Rigos for their assistance with some of the computational work.

REFERENCES

1. S. A. Safran and N. A. Clark, eds. *Physics of Complex and Supermolecular Fluids* (Wiley-Interscience, New York, 1987).
2. D. J. Evans and R. O. Watts, *Chem. Phys.* **48**:321 (1980).
3. G. Bossis and J. F. Brady, *J. Chem. Phys.* **80**:5141 (1984).
4. G. Bossis and J. F. Brady, *J. Chem. Phys.* **91**:1866 (1989).
5. J. F. Brady and G. Bossis, *J. Fluid Mech.* **155**:105 (1985).
6. L. V. Woodcock, *Chem. Phys. Lett.* **111**:455 (1984); *Phys. Rev. Lett.* **54**:1513 (1985).
7. D. M. Heyes, *J. Non-Newtonian Fluid Mech.* **27**:47 (1988).
8. D. M. Heyes, *Phys. Lett. A* **132**:399 (1988).
9. M. Doi and D. Chen, *J. Chem. Phys.* **90**:5271 (1989).
10. G. Wilemski, Colloidal Dynamics Simulations of Rheology and Stability of Concentrated Fuel Slurries, Final Report to AFOSR, PSI-2009/TR-666, Physical Sciences Inc., NTIS/AD-A182462/2 (1987).
11. W. B. Russel, *J. Rheol.* **24**:287 (1980); *The Dynamics of Colloidal Systems* (University of Wisconsin Press, Madison, Wisconsin, 1987).
12. D. L. Ermak and J. A. McCammon, *J. Chem. Phys.* **69**:1352 (1978).
13. M. Fixman, *J. Chem. Phys.* **69**:1527, 1538 (1978); *Macromolecules* **14**:1710 (1981).
14. G. C. Ansell, E. Dickinson, and M. Ludvigsen, *J. Chem. Soc. Faraday Trans. 2* **81**:1269 (1985).
15. A. Lees and S. F. Edwards, *J. Phys. C* **5**:1921 (1972).
16. W. G. Hoover and W. T. Ashurst, in *Theoretical Chemistry*, Vol. 1 (Academic, New York, 1975); D. J. Evans, *Mol. Phys.* **37**:1745 (1979).
17. H. C. Hamaker, *Physica* **4**:1058 (1937).
18. R. H. Ottewill and T. Walker, *Kolloid Z. Z. Polym.* **227**:108 (1968).
19. R. J. R. Cairns, W. van Megen, and R. Ottewill, *J. Colloid. Interface Sci.* **79**:511 (1981).
20. E. J. W. Verwey and J. Th. G. Overbeek, *The Theory of the Stability of Lyophobic Colloids* (Elsevier, Amsterdam, 1948).
21. W. van Megen and I. Snook, *Faraday Disc. Chem. Soc.* **76**:151 (1983).
22. H. J. M. Hanley, J. C. Rainwater, N. A. Clark, and B. J. Ackerson, *J. Chem. Phys.* **79**:4448 (1983).
23. J. J. Erpenbeck, *Phys. Rev. Lett.* **52**:1333 (1984).
24. D. M. Heyes, *J. Chem. Soc. Faraday Trans. 2* **82**:1365 (1986).
25. D. J. Evans and G. P. Morriss, *Phys. Rev. Lett.* **56**:2172 (1986).
26. R. Cook and G. Wilemski, unpublished.